

Synthesis and physical properties of CeRu₂As₂ and CeIr₂As₂

Kangqiao Cheng¹, Xiaobo He¹, Haiyang Yang², Binjie Zhou¹, Yuke Li^{2,*} and Yongkang Luo^{1†}

¹Wuhan National High Magnetic Field Center and School of Physics,
Huazhong University of Science and Technology, Wuhan 430074, China; and

²Department of Physics and Hangzhou Key Laboratory of Quantum Matters,
Hangzhou Normal University, Hangzhou 311121, China.

(Dated: March 13, 2024)

We studied the physical properties of two Kondo-lattice compounds, CeRu₂As₂ and CeIr₂As₂, by a combination of electric transport, magnetic and thermodynamic measurements. They are of ThCr₂Si₂-type and CaBe₂Ge₂-type crystalline structures, respectively. CeRu₂As₂ shows localized long-range antiferromagnetic ordering below $T_N=4.3$ K, with a moderate electronic Sommerfeld coefficient $\gamma_0=35$ mJ/mol·K². A field-induced metamagnetic transition is observed near 2 T below T_N . Magnetic susceptibility measurements on aligned CeRu₂As₂ powders suggest that it has an easy axis and that the cerium moments align uniaxially along **c** axis. In contrast, CeIr₂As₂ is a magnetically nonordered heavy-fermion metal with enhanced $\gamma_0>300$ mJ/mol·K². The initial onset Kondo temperatures of the two compounds are respectively 6 K and 30 K. We discuss the role of the crystal structure to the strength of Kondo coupling. This work provides two new dense Kondo-lattice materials for further investigations on electronic correlation, quantum criticality and heavy-electron effects.

I. INTRODUCTION

The hybridization (J_{cf}) between conduction (*c*) electrons and more localized *f* electrons in Kondo-lattice compounds simultaneously yields two competing phenomena: the Ruderman-Kittel-Kasuya-Yosida (RKKY) interaction[1–3] and the Kondo effect[4, 5]. While the RKKY interaction mediates the magnetic exchange between local moments and stabilizes a long-range magnetic ordering, the consequence of Kondo effect is to screen and quench the local moments. Depending on the strength of J_{cf} , the ground state of Kondo lattices varies from localized magnetic ordered regime for small J_{cf} , heavy-fermion regime for moderate J_{cf} to intermediate-valence regime for large J_{cf} .

“Ce-122” refers to a big family of Kondo-lattice compounds. It is mainly comprised of two types of tetragonal crystalline structures: the ThCr₂Si₂-type (I4/*mmm*, No. 139) and CaBe₂Ge₂-type (P4/*nmm*, No. 129). We show their crystalline structures in Fig. 1(a). The discovery of superconductivity in K-doped BaFe₂As₂ rekindled the interest in the ThCr₂Si₂ structure[6]. In this structure, two vertically inverted CrSi layers are alternately sandwiched with Th ions embedded in between. Historically, ThCr₂Si₂ structure was also well-known for hosting a number of Kondo-lattice materials (see reviews [7–9]), including CeCu₂Si₂ - the first heavy-fermion superconductor[10], URu₂Si₂ - hidden order superconductor[11], YbRh₂Si₂ - Kondo breakdown quantum critical point[12] *et al.* The CaBe₂Ge₂-type structure is relatively less famous. In this structure, the Be and Ge sites are interchanged in every other layer, and interlayer couplings can be bridged by Be-Ge bonding, which renders a more three-dimensional network than ThCr₂Si₂. Some examples are CeRh₂P₂[13], CeNi₂As₂[14], CeIr₂Si₂[15] *etc.* Note that CeNi₂As₂ can

crystallize in both structures[14, 16, 17]. For whatever ThCr₂Si₂- or CaBe₂Ge₂-type Ce-122, the Ce-4*f* electrons interact with the conduction electrons donated by CrSi or BeGe layers, and such a *c-f* hybridization builds up a natural platform to investigate Kondo effect and electronic correlations. A variety of interesting emergent states have been observed in Ce-122 compounds, *e.g.* metamagnetism, heavy-fermion, non-Fermi liquid, quantum critical point (QCP), and unconventional superconductivity[10, 17–22], the mechanisms of which remain controversial. In particular, local centrosymmetry is broken in CaBe₂Ge₂-type Ce-122, making them candidates to look for new non-centrosymmetric heavy-fermion superconductors. Extensive material bases are required in this field.

In this paper, we study two Ce-122 Kondo-lattice compounds, CeRu₂As₂ and CeIr₂As₂. The ThCr₂Si₂-type CeRu₂As₂ is a new material. The synthesis of CaBe₂Ge₂-type CeIr₂As₂ has been reported by Pfannenschmidt *et al*[23], but its physical properties have not been well studied. Our work reveals that CeRu₂As₂ is a 4*f*-electron localized antiferromagnet with Néel temperature $T_N=4.3$ K and a moderate Sommerfeld coefficient $\gamma=35$ mJ/mol·K², whereas CeIr₂As₂ is magnetically nonordered heavy-fermion metal with enhanced Sommerfeld coefficient $\gamma_0>300$ mJ/mol·K². The initial onset Kondo temperatures of the two compounds are respectively 6 K and 30 K. These results place them in the regimes of magnetic ordered with small J_{cf} and heavy-fermion with moderate J_{cf} , respectively.

II. EXPERIMENTAL DETAILS

Polycrystalline CeRu₂As₂ and CeIr₂As₂ samples were synthesized by the method of solid-state reaction. High-

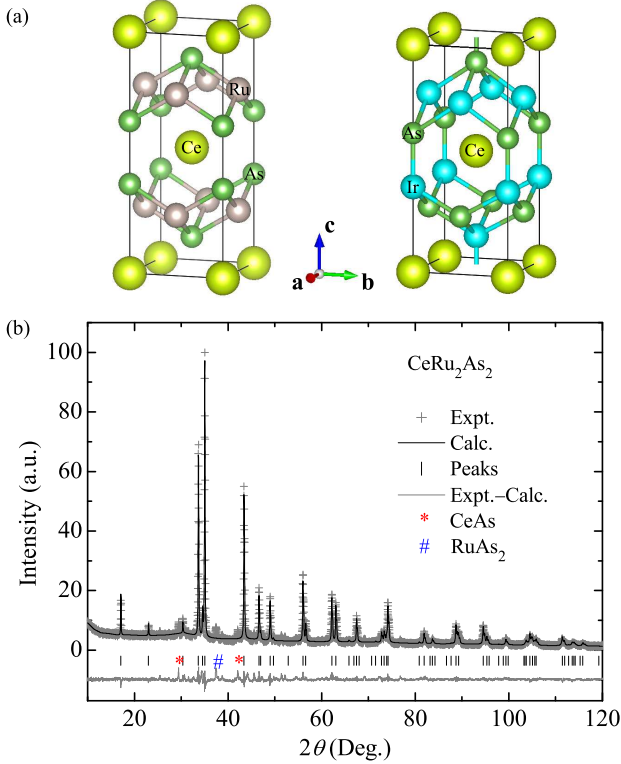


FIG. 1. (a) Crystalline structure of ThCr₂Si₂-type CeRu₂As₂ (left) and CaBe₂Ge₂-type CeIr₂As₂ (right). (b) Rietveld refinement of CeRu₂As₂ XRD pattern.

purity Ce, Ru, Ir and As were used as starting materials. First, CeAs, RuAs and IrAs were prepared by reacting As powders with Ce, Ru and Ir powders at 973 K, 1073 K and 1273 K respectively for 24 hours. Then, powders of CeAs, RuAs and Ru were weighted according to the stoichiometric ratio, thoroughly ground and pressed into a pellet under a pressure of 600 MPa in an argon-filled glove box. The pellet was packed into an alumina crucible and sealed into an evacuated quartz tube, which was then slowly heated to 1323 K and kept at that temperature for 48 hour. After that, the resultant was re-ground and re-sintered for two more times to achieve a good homogeneity. The synthesis for CeIr₂As₂ was essentially similar, while the sintering temperature was at 1373 K. The non-4*f* analogs LaRu₂As₂ and LaIr₂As₂ were also grown, in the same method.

Powder x-ray diffraction (XRD) patterns were recorded at room temperature on a PANalytical X-ray diffractometer with Cu Kα radiation. Electrical resistivity was measured by standard four-probe method in a physical property measurement system (PPMS-9, Quantum Design), which was also used for the specific heat measurements. Magnetization measurements were performed using a magnetic property measurement system (MPMS-VSM, Quantum Design). The measurements

were made after a zero-field-cooling (ZFC) process.

III. RESULTS AND DISCUSSION

The crystalline structures of CeRu₂As₂ and CeIr₂As₂ are shown in Fig. 1. For the new compound CeRu₂As₂, we performed the Rietveld refinement to the XRD. The peaks are well indexed to the tetragonal ThCr₂Si₂-type structure, except for a little impurity phase of CeAs and RuAs₂. The best fitting parameters are $a=4.1696(5)$ Å, $c=10.3868(7)$ Å, and the atomic coordinate of As (0, 0, 0.3692(4)). More details about the structural parameters of CeRu₂As₂ and CeIr₂As₂ can be found in Table I. The lengths of *a*- and *c*-axes of CeIr₂As₂ obtained in this work are close to but a little smaller than those in literature[23]. The Ir-As bonding ($d_{\text{Ir-As}}=2.33$ Å) between adjacent IrAs layers makes *c*-axis much shorter than in CeRu₂As₂ ($d_{\text{As-As}}=2.72$ Å).

TABLE I. Crystallographic parameters of CeRu₂As₂ from the Rietveld refinement to the Powder X-ray Diffractions at 300 K. The data of CeIr₂As₂ are also shown for comparison.

Compounds	CeRu ₂ As ₂	CeIr ₂ As ₂
Space group	<i>I</i> 4/ <i>mmm</i>	<i>P</i> 4/ <i>mmm</i>
<i>a</i> (Å)	4.1696(5)	4.2865(6)
<i>c</i> (Å)	10.3868(7)	9.8849(9)
<i>V</i> (Å ³)	180.580	181.625
<i>Z</i>	2	2
ρ (g/cm ³)	9.050	12.332
<i>R</i> _{wp} (%)	9.36	11.57

Figure 2(a-b) show the temperature dependence of magnetic susceptibility ($\chi=M/B$) of polycrystalline CeRu₂As₂ and CeIr₂As₂. For temperature above 150 K, χ of both compounds obey standard Curie-Weiss formula, $\chi(T)=\frac{C}{T-\theta_W}$, where θ_W is the Weiss temperature. The fittings yield the effective moment $\mu_{\text{eff}}=2.50$ and $2.56 \mu_B$ for CeRu₂As₂ and CeIr₂As₂, respectively, very close to that of a free Ce³⁺ ion, $2.54 \mu_B$. This implies that the Ru and Ir ions are essentially nonmagnetic. The derived θ_W is -51 K for CeRu₂As₂, suggestive of antiferromagnetic correlation among Ce moments. A hump is seen near 80 K in CeIr₂As₂, which makes χ less temperature-dependent at low temperature. Similar behavior was also seen in CeCoIn₅ and CeIrIn₅[24], which is probably due to the crystalline electric field (CEF) effect, see below. For comparison, the magnetic susceptibility of CeIr₂P₂ (data reproduced from Ref. [23]) is also shown in Fig. 2. Pfannenschmidt *et al* placed CeIr₂P₂ in the regime of intermediate-valence, based on the Pauli-paramagnetic-like $\chi(T)$. Apparently, the “chemical pressure” effect of As-P substitution greatly enhances the *c-f* hybridization, and the 4*f* electrons become delocalized in CeIr₂P₂. At low temperature, the most promi-

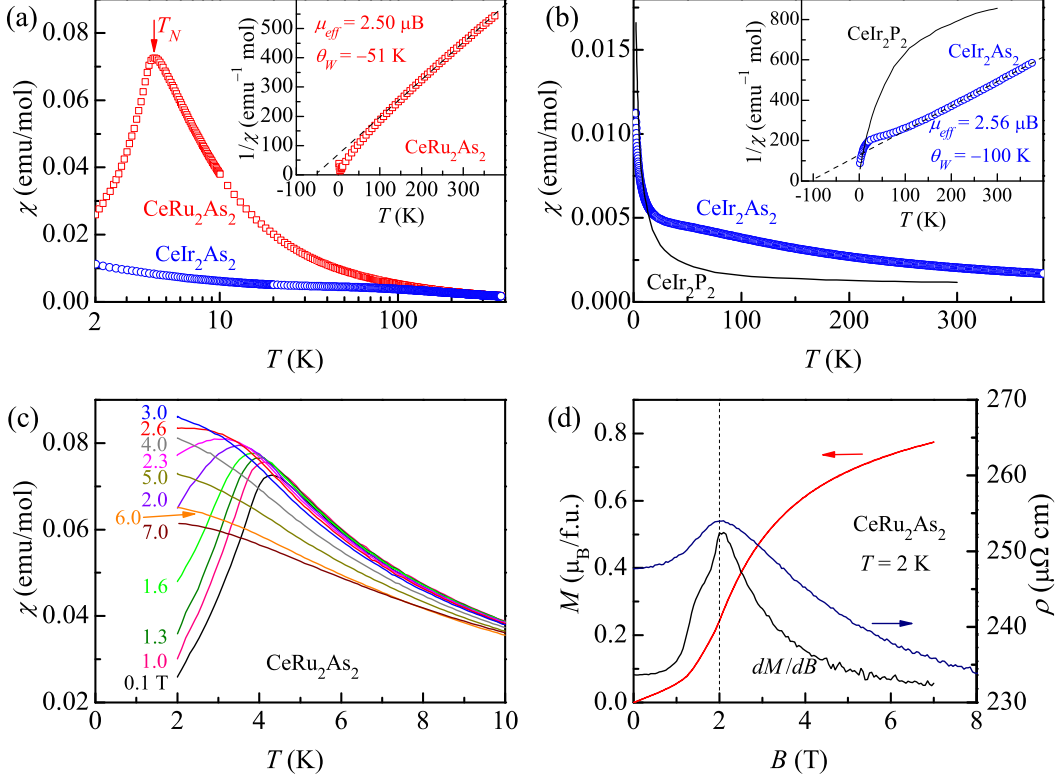


FIG. 2. (a-b) Temperature dependent magnetic susceptibility of polycrystalline CeRu_2As_2 and CeIr_2As_2 . CeRu_2As_2 undergoes an AFM transition at $T_N = 4.3$ K. The insets display the Curie-Weiss fittings. The curve of CeIr_2P_2 (black line) reproduced from Ref. [23] is shown for comparison. (c) Evolution of the AFM peak in $\chi(T)$ of CeRu_2As_2 under various fields. (d) Field dependent magnetization (left), resistivity (right) and derivative susceptibility (dM/dB) of CeRu_2As_2 at 2 K.

nent feature of CeRu_2As_2 is that $\chi(T)$ displays a sharp peak at 4.3 K, manifesting an antiferromagnetic (AFM) transition which will be studied further. No anomaly is seen in CeIr_2As_2 at low T ; the slight increase in χ is probably due to some magnetic impurities (CeAs). We should point out that the fitted θ_W from the high- T region is ~ -110 K for CeIr_2As_2 , much larger than that of CeRu_2As_2 . Since CeIr_2As_2 does not show any magnetic ordering, this enhanced θ_W is likely promoted by the Kondo effect. Further transport and specific heat measurements suggest that CeIr_2As_2 sits much closer to a QCP.

In Fig. 2(c), we display $\chi(T)$ of CeRu_2As_2 under different magnetic fields. As field increases, the peak in $\chi(T)$ is gradually suppressed, and meanwhile the peak position also moves to lower temperature, characteristic of an AFM transition. For field at about 2.6 T, the peak disappears, and $\chi(T)$ saturates at low temperature. Further increasing B , the value of magnetic susceptibility decreases systematically, and no clear anomaly is seen in $\chi(T)$ only except for a trend of saturation at low T . Such an evolution with field typically entails a field-induced metamagnetic transition, as observed

in many cerium compounds[17, 25]. Since Ce^{3+} has a small de Gennes factor[26], the magnetic exchange coupling between cerium moments are generally weak, thus, the magnetic moments can be reoriented by a moderate field. This is indeed the case in CeRu_2As_2 . In Fig. 2(d), we present isothermal field dependent magnetization and derivative susceptibility (dM/dB) at 2 K. Under low field, the magnetization increases linearly. A speed-up is visible for field larger than 1 T, and finally tends to saturate above 4 T. This trend is more clearly seen in dM/dB that peaks near 2 T. Similar metamagnetic transition was interpreted as a spin-flop in CeNi_2As_2 where the magnetic moments are uniaxially aligned along c and a tiny hysteresis is seen near the metamagnetic transition[17]. In CeRu_2As_2 , the hysteresis is negligible, probably due to the polycrystalline sample.

To further study the magnetic anisotropy of CeRu_2As_2 , we measured the susceptibility of field-aligned powders. The polycrystalline sample is thoroughly ground into powders (This process is carried out carefully in a glove box), and mixed with Stycast 1266 epoxy with a small weight ratio ~ 0.2 so that the grains are well isolated by epoxy[27]. The mixture is then placed in a

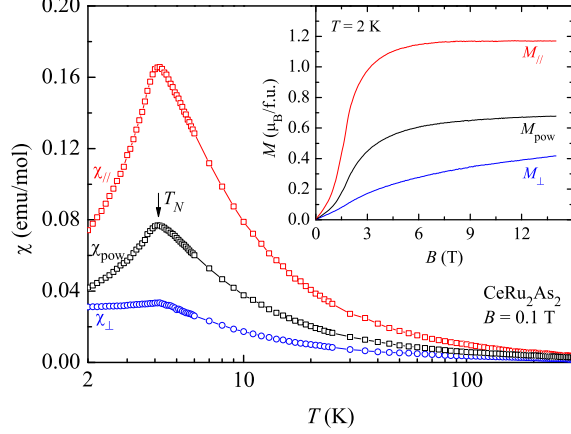


FIG. 3. Temperature dependence of χ_{\parallel} and χ_{\perp} measured from aligned CeRu_2As_2 powders. The inset shows the isothermal field dependent magnetization. \parallel and \perp are with respect to the aligning field \mathbf{B}_{al} . Seeing Appendix. The results for unaligned powders (χ_{pow}) are shown for comparison.

strong aligning field (\mathbf{B}_{al}) of 14 T at 300 K in PPMS and held motionless for 12 hours before the Stycast is completely cured. The magnetic susceptibility for parallel (χ_{\parallel}) and perpendicular (χ_{\perp}) to \mathbf{B}_{al} are shown in Fig. 3 as a function of T . (Refer to Appendix for more details.) The important findings are: (i) χ_{\perp} is much smaller than χ_{\parallel} , indicative of strong magnetic anisotropy. In particular, we notice the value of χ_{\perp} is less than a half of χ_{\parallel} over the full range 2-300 K, for instance, at 300 K, $\chi_{\parallel} = 3.65 \times 10^{-3}$ emu/mol, and $\chi_{\perp} = 1.66 \times 10^{-3}$ emu/mol. This suggests that the compound has an easy axis, rather than easy plane, because for the latter case, $\chi_{\parallel} = \chi_{a,b}$, and $\chi_{\perp} = (\chi_{a,b} + \chi_c)/2$ (Seeing Appendix); $\chi_{\perp} < \chi_{\parallel}/2$ is not likely for cerium-contained compounds. (ii) At low temperature, a sharp peak is seen at T_N in χ_{\parallel} , characteristic of an AFM transition. In contrast, the peak in χ_{\perp} is very shallow, and the susceptibility tends to saturate below T_N . These features are highly suggestive that in the AFM state the Ce moments are uniaxially along the easy axis. (iii) The inset to Fig. 3 shows field dependent magnetization of aligned powders at 2 K. M_{\parallel} increases with field rapidly and saturates at $1.17 \mu_B$ under high magnetic field. The metamagnetic transition is obviously seen in M_{\parallel} , even sharper than in unaligned powders (M_{pow}). M_{\perp} is much smaller than M_{\parallel} and keeps increasing at 14 T. A little sign of metamagnetic transition is also visible in M_{\perp} , which probably arises from a small portion of unaligned powders. In light of these observations, it is reasonable to propose \mathbf{c} as the easy axis of CeRu_2As_2 , and below T_N the magnetic moments also align antiferromagnetically along \mathbf{c} . This makes a field-induced spin-flop possible. In fact, the dM/dB in Fig. 2(d) shows a small shoulder before 2 T, which po-

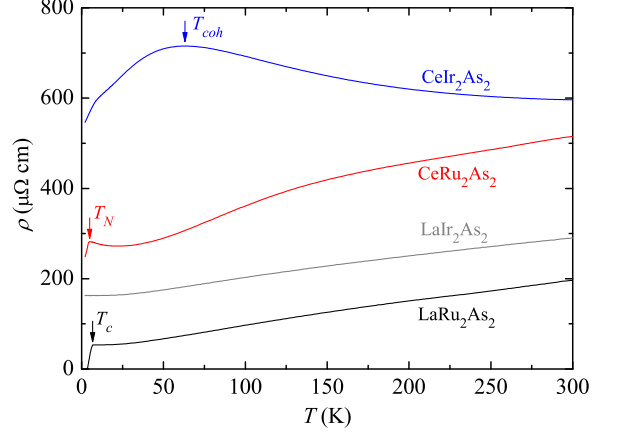


FIG. 4. Temperature dependent electric resistivity of CeRu_2As_2 , CeIr_2As_2 , LaRu_2As_2 and LaIr_2As_2 .

tentially points to a secondary transition prior to the polarized paramagnetic state. Given an easy-axis antiferromagnet, this secondary transition might be a signature for an intermediate spin-flop phase. Of course, to get a precise magnetic structure, high-quality single crystals and microscopic measurements like neutron scattering experiments are needed. Crystalline electric field (CEF) effect often plays a key role to such a magnetic anisotropy in cerium compounds.

The resistivity (ρ) of CeRu_2As_2 , CeIr_2As_2 and their La-counterparts are presented in Fig. 4. A previous work on LaRu_2As_2 by Guo *et al* has revealed metallic behavior and a superconducting transition at $T_c = 7.8$ K [28], and these features are well reproduced in the current work. For CeRu_2As_2 , $\rho(T)$ shows a hump around 150 K, which should be a consequence of CEF splitting of Ce^{3+} $j=5/2$ multiplet. $\rho(T)$ slightly turns up below 22 K, and then decreases sharply below 4.3 K, reminiscent of reduction in spin scattering due to the formation of long-range AFM ordering. LaIr_2As_2 behaves like a simple metal, say, upon cooling down, $\rho(T)$ decreases almost linearly above 100 K, and then tends to flatten by showing some T^2 -like behavior at low temperature, characteristic of Fermi liquid. The large residual resistivity ρ_0 is probably because of the sample quality. In contrast, CeIr_2As_2 exhibits the typical dense Kondo behavior (see *e.g.* CeIrIn_5 [29, 30]): $\rho(T)$ initially increases as T decreases, and then turns down rapidly after passing through a broad peak near $T_{\text{coh}} = 63$ K. T_{coh} designates a crossover from incoherent Kondo scattering regime for $T > T_{\text{coh}}$ where Ce moments behaves like separate single-ion impurities to the coherent Kondo scattering regime for $T < T_{\text{coh}}$ where the Ce-4*f* electrons develop strongly-correlated bands. At low temperature, $\rho(T)$ keeps decreasing linearly down to 2 K, the base temperature of our measurements, without restoring any signature of Fermi-liquid behavior. This places CeIr_2As_2 in

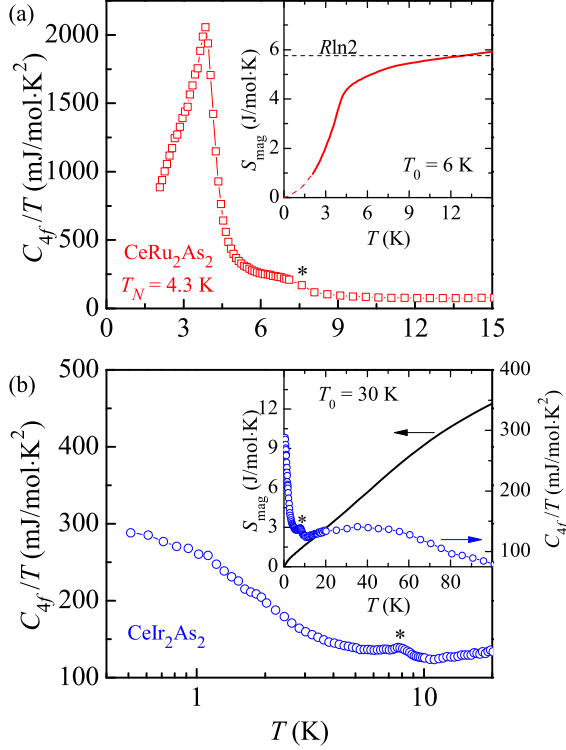


FIG. 5. The 4f-electron contribution to specific heat divided by temperature, C_{4f}/T , as a function of T of CeRu_2As_2 (a) and CeIr_2As_2 (b). The insets show the magnetic entropy derived by integrating C_{4f}/T over T . A broad maximum seen in C_{4f}/T of CeIr_2As_2 near 40 K indicates ~ 90 K of the first CEF splitting, which is consistent with what is seen in $\chi(T)$. The “*” in both panels designate the anomalies due to CeAs impurity.

a regime of non-Fermi liquid or “strange metal” [7] which is usually observed in the vicinity of a quantum critical point [12, 31–34]. Sub-Kelvin measurements are needed in the future to further clarify this issue.

For CeRu_2As_2 , we also took a field dependent resistivity measurement at 2 K (below T_N), as shown in Fig. 2(d). Under low field, ρ increases with field, because external magnetic field disturbs the long-range AFM ordering and causes more spin scattering. A maximum is seen in $\rho(B)$ at 2 T, and after that, the resistivity decreases again. The critical field 2 T is coincident with the field at which $M(B)$ shows the largest slope and dM/dB peaks. Further increasing B , spin scattering is reduced as the moments are gradually polarized, and thus the resistivity decreases.

Turning now to the specific heat. For both CeRu_2As_2 and CeIr_2As_2 , we respectively subtract the specific heat of LaRu_2As_2 (measured under field of 1 T) and LaIr_2As_2 , and the resultants are the contribution from 4f electrons, C_{4f} . Fig. 5(a) shows C_{4f}/T of CeRu_2As_2 as a

function of T . A λ -shape peak is clearly seen at the transition temperature T_N , manifesting a second-order phase transition. A small sub-structure is seen between 6–9 K, which should be from some CeAs impurity that undergoes an AFM transition at 7.6 K [35]. The Sommerfeld coefficient γ_0 estimated from the paramagnetic state is 35 $\text{mJ/mol}\cdot\text{K}^2$, in line with the well localized and ordered 4f electrons. We calculated the magnetic entropy (S_{mag}) by integrating C_{4f}/T over T . For the low temperature part, we have linearly extrapolated the C_{4f}/T to $T \rightarrow 0$ limit to ensure $S_{\text{mag}}(0)=0$, and the result is plotted in the inset to Fig. 5(a). The entropy gain is about 73% $R\ln 2$ at T_N , and fully recovers $R\ln 2$ at 12 K. The initial onset Kondo temperature can be estimated as $T_0 \approx 6$ K through a widely accepted criterion $S_{\text{mag}}(T_0/2) = 0.4R\ln 2$ [36]. For CeIr_2As_2 , C_{4f}/T turns up logarithmically at low temperature, and tends to level off below 1 K. This suggests that the Fermi liquid behavior likely restores at low temperature with greatly enhanced quasiparticle effective mass and Sommerfeld coefficient $\gamma_0 > 300 \text{ mJ/mol}\cdot\text{K}^2$. Such kind of behavior is usually seen in systems beyond but close to a QCP [37–39]. The estimated T_0 is about 30 K, much larger than that of CeRu_2As_2 , demonstrating stronger Kondo coupling. We should also mention that C_{4f}/T displays a broad maximum near 40 K, see the right frame of the inset to Fig. 5(b). Such a broad peak arises from the Schottky anomaly which is a consequence of CEF splitting. The six-degenerated $j=5/2$ multiplet splits into three doublets in the presence of tetragonal CEF. The energy difference between the first excited and ground doublets is expected to be ~ 90 K in this case, which agrees well with the hump observed in magnetic susceptibility [cf Fig. 2(b)].

These physical properties above enable us to place CeRu_2As_2 and CeIr_2As_2 respectively in the regime of magnetic ordered for small J_{cf} and heavy-fermion for moderate J_{cf} . Aside from them, CeIr_2P_2 sits in the intermediate-valence regime with strong J_{cf} . Firstly, it is worthwhile to make a rough estimate of cerium valence through the bond-valence theory. The original idea was proposed by Brown [40, 41], and the valence of an ion in the compound is a function of the bond lengths d_{ij} ,

$$V_i = \sum_j \nu_{ij}, \quad (1)$$

where ν_{ij} can be expressed in terms of d_{ij} [42],

$$\nu_{ij} = \exp[(R_{ij} - d_{ij})/b]. \quad (2)$$

Here b is commonly taken to be a “universal” constant close to 0.37 Å, while R_{ij} is called bond-valence parameter and is taken as 2.78 Å for Ce-As bonding and 2.70 Å for Ce-P bonding [42]. According to the crystalline parameters, we get the cerium valences +2.27, +2.28 and +2.53 for CeRu_2As_2 , CeIr_2As_2 and CeIr_2P_2 , respectively.

These values apparently are underestimated as compared to $\text{Ce}^{3+/4+}$, because we only take into account the Ce-As(P) bonding with nearest neighbour. However, what are important here are: (i) the cerium valence in CeIr_2P_2 is much higher than in CeIr_2As_2 , in line with the fact that CeIr_2P_2 has an intermediate valence; (ii) the calculated cerium valences are essentially the same in CeRu_2As_2 and CeIr_2As_2 . This indicates that the transition metal is crucial to the physical properties of CeTm_2As_2 . Indeed, $5d$ orbitals are more extended in space than $4d$ orbitals, and this makes the c - f hybridization more effective in CeIr_2As_2 . Apart from this, as we already mentioned, the CaBe_2Ge_2 -type CeIr_2As_2 has the interlayer Ir-As bonding, and this results in a three-dimensional Ir-As network, and correspondingly, Kondo coupling is more efficient. A more straightforward case is CeNi_2As_2 , which has both types of crystal structures[14]. While the ThCr_2Si_2 -type CeNi_2As_2 is an antiferromagnet with $T_N \approx 5$ K[17], the CaBe_2Ge_2 -type CeNi_2As_2 is nonmagnetic due to Kondo effect[16]. We argue that for these two reasons, the CaBe_2Ge_2 -type CeIr_2As_2 exhibits much stronger Kondo effect and electronic correlation than the ThCr_2Si_2 -type CeRu_2As_2 .

IV. CONCLUSIONS

To summarize, we investigated the physical properties of two Ce-122 Kondo lattice compounds, ThCr_2Si_2 -type CeRu_2As_2 and CaBe_2Ge_2 -type CeIr_2As_2 . We find that CeRu_2As_2 is a local-moment antiferromagnet with Néel temperature $T_N = 4.3$ K, Sommerfeld coefficient $\gamma_0 = 35$ mJ/mol·K² and initial onset Kondo temperature $T_0 \approx 6$ K. The cerium moments are assumed to be uniaxially aligned along \mathbf{c} which is also proposed as the easy-axis. CeIr_2As_2 appears to reside on the nonmagnetic side of a quantum critical point, exhibiting heavy-electron effect with enlarged $\gamma_0 > 300$ mJ/mol·K² and $T_0 \approx 30$ K. This work, therefore, provides two new dense Kondo-lattice materials for further studying electronic correlation, quantum criticality and heavy-electron effects. High-quality single crystals are highly needed in the future.

ACKNOWLEDGMENTS

The authors acknowledge Joe D. Thompson and Jinke Bao for helpful discussions. Y. Luo acknowledges 1000 Youth Talents Plan of China. Y. Li is supported by National Natural Science Foundation of China (Grant No. U1932155).

APPENDIX: Magnetic susceptibility for aligned powders

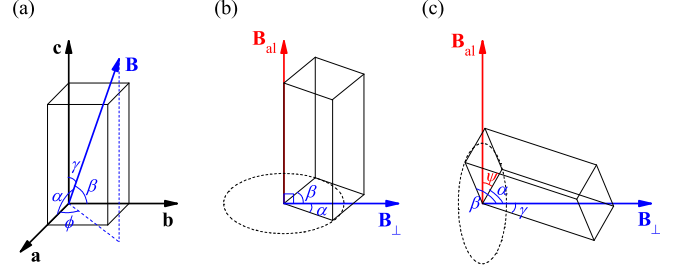


FIG. A1. (a) External magnetic field \mathbf{B} applied in an arbitrary direction with respect to the *tetragonal* unit cell. α , β and γ are the angles between \mathbf{B} and the principal axes, and ϕ is the angle spanned by \mathbf{a} and the projection of \mathbf{B} in \mathbf{ab} plane. (b) For the easy-axis case, \mathbf{c} is along the aligning field \mathbf{B}_{al} . (c) For the easy-plane case, \mathbf{B}_{al} is inside \mathbf{ab} plane, and \mathbf{c} is perpendicular to \mathbf{B}_{al} . \mathbf{B}_{\perp} (\mathbf{B}_{\parallel} , not shown) is the field applied perpendicular (parallel) to \mathbf{B}_{al} to measure m_{\perp} (m_{\parallel}).

To start with, we deduce the formulas of magnetic susceptibility of polycrystalline powders. Assuming an arbitrary magnetic field \mathbf{B} is applied to a tetragonal unit cell (e.g. CeRu_2As_2), the direction of field is characterized by α , β and γ as shown in Fig. A1(a). The magnetic susceptibility in such configuration is $\chi(\alpha, \beta, \gamma) = \chi_a \cos^2 \alpha + \chi_b \cos^2 \beta + \chi_c \cos^2 \gamma$ [43]. Note that $\chi_a = \chi_b$ for tetragonal symmetry. Taking the powder average, we derive the susceptibility for a bulk polycrystal

$$\chi_{\text{pow}} = \frac{\int \int \chi(\alpha, \beta, \gamma) \sin \gamma d\gamma d\phi}{\int_0^{2\pi} \int_0^{\pi} \sin \gamma d\gamma d\phi} = \frac{\chi_a + \chi_b + \chi_c}{3}, \quad (\text{A1})$$

where ϕ is the angle between \mathbf{a} and the projection of \mathbf{B} in \mathbf{ab} plane.

Now considering that the powder is aligned by an aligning field \mathbf{B}_{al} :

- For an easy-axis case [Fig. A1(b)], \mathbf{c} will be aligned to \mathbf{B}_{al} , and one easily finds $\chi_{\parallel} = \chi_c$, while $\chi_{\perp} = \chi_{a,b}$. Here, the notations \parallel and \perp are with respect to \mathbf{B}_{al} .
- For an easy-plane case [Fig. A1(c)], \mathbf{ab} plane will be parallel with \mathbf{B}_{al} , while \mathbf{c} lays inside the plane perpendicular to \mathbf{B}_{al} . The angle between \mathbf{a} and \mathbf{B}_{al} is named ψ . In this case, $\chi_{\parallel} = \chi_{a,b}$, while χ_{\perp} is

$$\chi_{\perp} = \frac{\int \int \chi(\alpha, \beta, \gamma) \sin \psi d\psi d\gamma}{\int_0^{2\pi} \int_0^{\pi} \sin \psi d\psi d\gamma} = \frac{\chi_{a,b} + \chi_c}{2}. \quad (\text{A2})$$

Eq. (A2) can be deduced, because $\cos \alpha = \sin \psi \sin \gamma$, and $\cos \beta = -\cos \psi \sin \gamma$. Interestingly, for both easy-axis and easy-plane cases,

$$\chi_{\parallel} + 2\chi_{\perp} = \chi_a + \chi_b + \chi_c = 3\chi_{\text{pow}}. \quad (\text{A3})$$

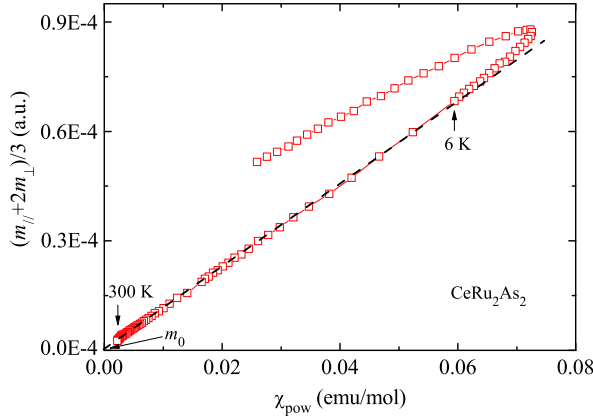


FIG. A2. $(m_{\parallel} + 2m_{\perp})/3$ vs. χ_{pow} with T as an implicit parameter. The slope is determined by the weight of aligned CeRu_2As_2 powders.

Eq. (A3) enables us to figure out the weight of aligned powders in the mixture. In Fig. A2 we plot $(m_{\parallel} + 2m_{\perp})/3$ vs. χ_{pow} where T is the implicit parameter. The plot shows good linearity for T above 6 K. The intercept of this linear scaling, m_0 , should be attributed to Stycast (which we assume is isotropic and temperature independent), and the slope is determined by the weight of the aligned powders. After subtracting m_0 from m_{\parallel} and m_{\perp} , and with the slope, we are able to convert magnetization into magnetic susceptibility, as shown in Fig. 3(a).

* yklee@hznu.edu.cn

† mpzsyk@gmail.com

- [1] M. A. Ruderman and C. Kittel, *Phys. Rev.* **96**, 99 (1954).
- [2] T. Kasuya, *Prog. Theor. Phys.* **16**, 45 (1956).
- [3] K. Yosida, *Phys. Rev.* **106**, 893 (1957).
- [4] J. Kondo, *Prog. Theor. Phys.* **32**, 37 (1964).
- [5] A. C. Hewson, *The Kondo Problem to Heavy Fermions* (Cambridge University Press, Cambridge, 1993).
- [6] M. Rotter, M. Tegel, and D. Johrendt, *Phys. Rev. Lett.* **101**, 107006 (2008).
- [7] G. R. Stewart, *Rev. Mod. Phys.* **73**, 797 (2001).
- [8] P. Misra, *Handbook of Metal Physics: Heavy-Fermion Systems* (Elsevier, Amsterdam, 2008).
- [9] C. Pfleiderer, *Rev. Mod. Phys.* **81**, 1551 (2009).
- [10] F. Steglich, J. Aarts, C. D. Bredl, W. Lieke, D. Meschede, W. Franz, and H. Schäfer, *Phys. Rev. Lett.* **43**, 1892 (1979).
- [11] T. T. M. Palstra, A. A. Menovsky, J. v. d. Berg, A. J. Dirkmaat, P. H. Kes, G. J. Nieuwenhuys, and J. A. Mydosh, *Phys. Rev. Lett.* **55**, 2727 (1985).
- [12] J. Custers, P. Gegenwart, H. Wilhelm, K. Neumaier, Y. Tokiwa, O. Trovarelli, C. Geibel, F. Steglich, C. Pepin, and P. Coleman, *Nature* **424**, 524 (2003).
- [13] R. Madar, P. Chaudouet, J. Senateur, S. Zemni, and D. Tranqui, *J. Less Common Met.* **133**, 303 (1987).
- [14] E. E. Ghadraoui, J. Pivan, R. Guérin, O. Pena, J. Padiou, and M. Sergent, *Mater. Res. Bull.* **23**, 1345 (1988).
- [15] K. Hiebl, C. Horvath, and P. Rogl, *J. Less Common Met.* **117**, 375 (1986).
- [16] H. Suzuki, H. Abe, H. Kitazawa, and D. Schmitt, *J. Alloys Comp.* **323-324**, 520 (2001).
- [17] Y. Luo, J. Bao, C. Shen, J. Han, X. Yang, C. Lv, Y. Li, W. Jiao, B. Si, C. Feng, J. Dai, G. Cao, and Z.-a. Xu, *Phys. Rev. B* **86**, 245130 (2012).
- [18] J. Flouquet, P. Haen, S. Raymond, D. Aoki, and G. Knebel, *Physica B* **319**, 251 (2002).
- [19] H. Q. Yuan, F. M. Grosche, M. Deppe, C. Geibel, G. Sparn, and F. Steglich, *Science* **302**, 2104 (2003).
- [20] F. Grosche, S. Julian, N. Mathur, and G. Lonzarich, *Physica B* **223-224**, 50 (1996).
- [21] R. Movshovich, T. Graf, D. Mandrus, J. D. Thompson, J. L. Smith, and Z. Fisk, *Phys. Rev. B* **53**, 8241 (1996).
- [22] Y. Luo, F. Ronning, N. Wakeham, X. Lu, T. Park, Z. A. Xu, and J. D. Thompson, *Proc. Natl. Acad. Sci. USA* **112**, 13520 (2015).
- [23] U. Pfannenschmidt, F. Behrends, H. Lincke, M. Eul, K. Schäfer, H. Eckert, and R. Pöttgen, *Dalton Trans.* **41**, 14188 (2012).
- [24] C. Petrovic, P. G. Pagliuso, M. F. Hundley, R. Movshovich, J. L. Sarrao, J. D. Thompson, Z. Fisk, and P. Monthoux, *J. Phys.: Condens. Matter* **13**, L337 (2001).
- [25] E. D. Mun, S. L. Bud'ko, A. Kreyssig, and P. C. Canfield, *Phys. Rev. B* **82**, 054424 (2010).
- [26] S. Blundell, *Magnetism in Condensed Matter* (Oxford University Press, 2001).
- [27] B.-L. Young, M. S. Rose, D. E. MacLaughlin, K. Ishida, O. O. Bernal, H. G. Lukefahr, K. Heuser, E. J. Freeman, and M. B. Maple, *Rev. Sci. Instrum.* **73**, 3038 (2002).
- [28] Q. Guo, B.-J. Pan, J. Yu, B.-B. Ruan, D.-Y. Chen, X.-C. Wang, Q.-G. Mu, G.-F. Chen, and Z.-A. Ren, *Sci. Bull.* **61**, 921 (2016).
- [29] C. Petrovic, R. Movshovich, M. Jaime, P. G. Pagliuso, M. F. Hundley, J. L. Sarrao, Z. Fisk, and J. D. Thompson, *EPL* **53**, 354 (2001).
- [30] Y. Takaesu, N. Aso, Y. Tamaki, M. Hedo, T. Nakama, K. Uchima, Y. Ishikawa, K. Deguchi, and N. K. Sato, *J. Phys: Conference Series* **273**, 012058 (2011).
- [31] H. v. Löhneysen, C. Pfleiderer, T. Pietrus, O. Stockert, and B. Will, *Phys. Rev. B* **63**, 134411 (2001).
- [32] T. Park, V. A. Sidorov, F. Ronning, J. X. Zhu, Y. Tokiwa, H. Lee, E. D. Bauer, R. Movshovich, J. L. Sarrao, and J. D. Thompson, *Nature* **456**, 366 (2008).
- [33] J. Custers, K.-A. Lorenzer, M. Müller, A. Prokofiev, A. Sidorenko, H. Winkler, A. M. Strydom, Y. Shimura, T. Sakakibara, R. Yu, Q. Si, and S. Paschen, *Nat. Mater.* **11**, 189 (2012).
- [34] Y. Luo, L. Pourouvkii, S. E. Rowley, Y. Li, C. Feng, A. Georges, J. Dai, G. Cao, Z. Xu, Q. Si, and N. P. Ong, *Nat. Mater.* **13**, 777 (2014).
- [35] T. Suzuki, Y. S. Kwon, S. Ozeki, Y. Haga, and T. Kasuya, *J. Mag. Mag. Mater.* **90-91**, 493 (1990).
- [36] P. Gegenwart, Q. Si, and F. Steglich, *Nat. Phys.* **4**, 186 (2008).
- [37] E. M. Brüning, C. Krellner, M. Baenitz, A. Jesche, F. Steglich, and C. Geibel, *Phys. Rev. Lett.* **101**, 117206 (2008).
- [38] Y. Luo, Y. Li, S. Jiang, J. Dai, G. Cao, and Z.-a. Xu, *Phys. Rev. B* **81**, 134422 (2010).

- [39] L. Wang, Z. Fu, J. Sun, M. Liu, W. Yi, C. Yi, Y. Luo, Y. Dai, G. Liu, Y. Matsushita, K. Yamaura, L. Lu, J.-G. Cheng, Y. feng Yang, Y. Shi, and J. Luo, [npj Quantum Materials](#) **2**, 36 (2017).
- [40] I. D. Brown, *Sturcture and Bonding in Crystals*, Vol. 2 (Academic Press, New York, 1981).
- [41] I. D. Brown and D. Altermatt, [Acta Cryst. B](#) **41**, 244 (1985).
- [42] N. E. Brese and M. O’Keeffe, [Acta Cryst. B](#) **47**, 192 (1991).
- [43] P. Boutron, [Phys. Rev. B](#) **7**, 3226 (1973).